Optics of photonic quasicrystals. Nat Photonics 7:177–187

Article *in* Nature Photonics · March 2013

DOI: 10.1038/nphoton.2012.343

3 authors, including:

Ajay Nahata
University of Utah
246 PUBLICATIONS **4,491** CITATIONS

SEE PROFILE

nature photonics

FOCUS | REVIEW ARTICLES

PUBLISHED ONLINE: 27 FEBRUARY 2013 | DOI: 10.1038/NPHOTON.2012.343

Optics of photonic quasicrystals

Z. Valy Vardeny[1]*, Ajay Nahata[2] and Amit Agrawal[3]

The physics of periodic systems are of fundamental importance and result in various phenomena that govern wave transport and interference. However, deviations from periodicity may result in higher complexity and give rise to a number of surprising effects. One such deviation can be found in the field of optics in the realization of photonic quasicrystals, a class of structures made from building blocks that are arranged using well-designed patterns but lack translational symmetry. Nevertheless, these structures, which lie between periodic and disordered structures, still show sharp diffraction patterns that confirm the existence of wave interference resulting from their long-range order. In this Review, we discuss the beautiful physics unravelled in photonic quasicrystals of one, two and three dimensions, and describe how they can influence optical transmission and reflectivity, photoluminescence, light transport, plasmonics and laser action.

The use of optical interference to enhance device performance is one of the most important tools in modern optics[1]. Important examples include photonic crystals[2–4], laser action in distributed feedback resonators[5,6], anomalous transmission through perforated metal films with subwavelength aperture arrays[7], coherent backscattering enhancement[8–10], image reconstruction[11] and Anderson localization of light[12,13]. Overwhelmingly, periodic structures are used for applications based on optical interference, largely because it has not been widely recognized that aperiodic structures, such as quasicrystals, can also provide similar functionalities. This is particularly relevant because the large variety of aperiodic structures, when compared with their periodic counterparts, can add significant flexibility and richness when engineering the optical response of devices in ways that have yet to be realized. In this Review, we describe the optical interference phenomena that occur in quasicrystalline structures.

It has now been shown that in addition to crystalline and amorphous materials, there exists a third intermediate class known as 'deterministic aperiodic' structures, which can be generated by a substitution rule based on two building blocks that exhibit long-range order but lack translational symmetry. All these structures exhibit properties of self-similarity. This class of structures can be further divided into two groups: quasicrystals (group 1) and all other deterministic aperiodic structures (group 2); quasicrystals therefore represent a special class of deterministic aperiodic structures. A more precise definition of quasicrystals in group 1 with dimensionality nD (n = 1, 2 or 3) is that in addition to their possible generation by a substitution process, they can also be formed from a partial projection of an appropriate periodic structure in a higher dimensional space mD, where $m > n$. In contrast, structures that are part of group 2 cannot be constructed in such a manner. In one dimension (1D), quasicrystal structures include the Fibonacci sequence *BABBA*… and the generalized Fibonacci sequence, for example. Aperiodic structures that differ from quasicrystals and belong to group 2 include Thue–Morse[14,15], Rudin–Shapiro[16] and period-doubling sequences[17]. All structures belonging to groups 1 and 2 show discrete Fourier components, although structures in group 2 exhibit much more complex Fourier properties than those in group 1[18].

The surprising discovery of quasicrystals by Shechtman *et al.*[19] in 1984, whereby a grown solid showed a sharp X-ray diffraction pattern of ten-fold rotational symmetry, took crystallographers and theoreticians in symmetry completely by surprise. A brilliant theoretical analysis by Levine and Steinhardt[20] elevated the scientific discussion of the finding and established the foundation of the new field of 'quasicrystals', which has revolutionized solid-state physics. Consequently, the 2011 Nobel Prize in Chemistry was awarded to Shechtman for the discovery of quasicrystals, and the 2011 Buckley Prize for Physics was given to Levine and Steinhardt for their theoretical analysis. The discovery of quasicrystals in condensed matter has also initiated a new field of research in photonics. The first example of an aperiodic system that possesses long-range order in the field of optics was described by Kohmoto *et al.*[21], who proposed a 1D quasicrystal structure (or photonic quasicrystal) that used dielectric multilayers to form the Fibonacci sequence (Fig. 1a). Subsequently, a broad range of photonic quasicrystals (group 1) and other deterministic aperiodic structures with long-range order (group 2) have been engineered and studied by optical means[17,22]. In all of these studies, interference has played a crucial role in the optical properties of each structure.

Although aperiodic structures in general lack translational symmetry[23], X-ray diffraction patterns of quasicrystals can be as sharp as those from regular periodic lattices[19]. The reason for this 'surprising' diffraction capability is that quasicrystals possess long-range order. Because the structure factor $F(\mathbf{k})$ of an object is the Fourier transform of its geometrical structure in real space, $F(\mathbf{k})$ contains a summation over 'atomic' positions $\mathbf{R}_n$, such that:

$$F(\mathbf{k}) = \lim_{N\to\infty} N^{-1} \sum_{\mathrm{R_n}} \exp(i\mathbf{k}\cdot\mathbf{R}_n)$$

It thus follows that saying a structure possesses long-range order is equivalent to saying that its $F(\mathbf{k})$ contains discrete Fourier components $F^{(i)}$, referred to as reciprocal vectors (RVs) in this Review, which can be used to describe the optical interference properties of the structure. Moreover, periodic and aperiodic structures have very different RVs in reciprocal space, which may be controlled by modifying the geometrical structure in real space[24].

In the following four sections, we restrict the discussion to aperiodic deterministic structures that are part of group 1 (that is, photonic quasicrystals). We summarize recent advances in demonstrating and utilizing the optical interference properties of a number of different photonic quasicrystals in various areas of optics. Examples include photoluminescence emission and super-radiance, anomalous transmission through plasmonic structures, wave propagation in waveguides and photonic crystals, and laser action. The photonic quasicrystals we discuss include 1D quasicrystalline

[1]Department of Physics and Astronomy, University of Utah, Salt Lake City, Utah 84112, USA. [2]Department of Electrical and Computer Engineering, University of Utah, Salt Lake City, Utah 84112, USA. [3]Department of Electrical Engineering and Computer Science, Syracuse University, Syracuse, New York 13244, USA. *e-mail: val@physics.utah.edu

NATURE PHOTONICS DOI: 10.1038/NPHOTON.2012.343

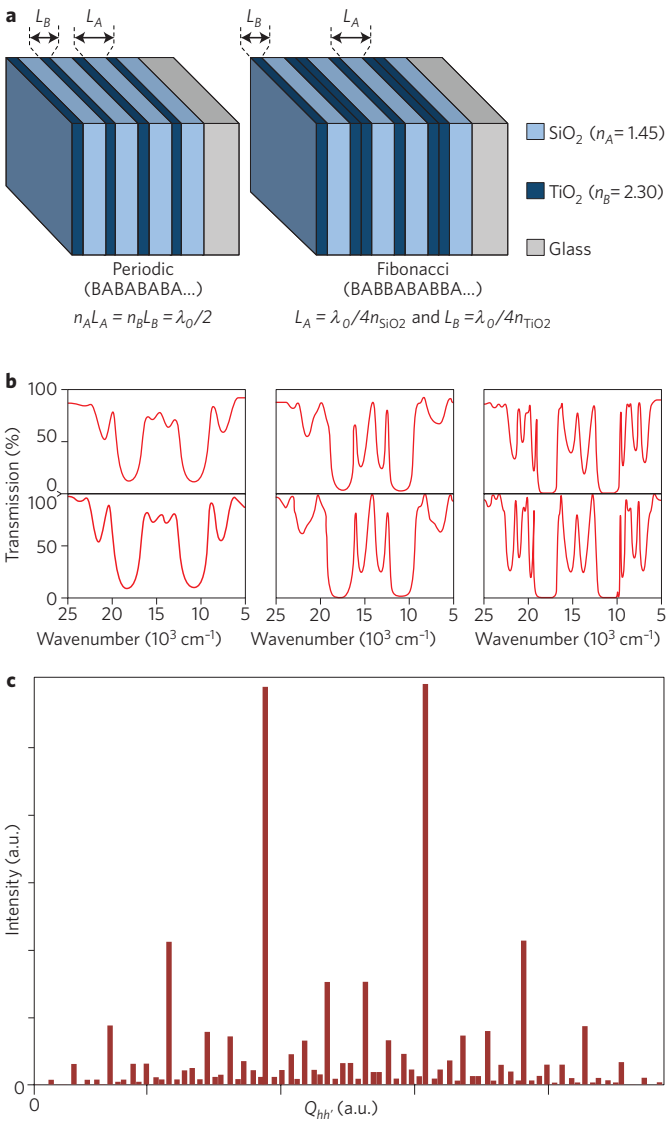

Figure 1 | Non-resonant 1D Fibonacci quasicrystalline structure. a, Schematic of a non-resonant multilayer Fibonacci structure composed of two dielectric layers (SiO_2 and TiO_2) of thicknesses L_A and L_B deposited using electron-beam evaporation on a glass substrate. The dielectric stacks are sandwiched between 6.5-mm-thick fused silica substrates. **b**, Optical transmission spectra (transmission versus wavenumber) for Fibonacci dielectric coating stacks S_6 to S_8, (where S_n is the nth Fibonacci sequence) that show the evolution of the transmission spectrum with the number of layers as S_n increases. The top (bottom) spectra show experimental (calculated) results. **c**, Fourier spectrum of a Fibonacci chain calculated with 987 inflation steps. Figure reproduced with permission from: **b**, ref. 25, © 1994 APL; **c**, ref. 23, © 1994 OUP.

structures such as dielectric multilayers and quantum-well (QW) multilayers (having mainly Fibonacci sequence), two-dimensional (2D) quasicrystalline structures (Penrose tiles, dodecagonal quasicrystals, quasicrystal approximates and 2D Fibonacci structures) and three-dimensional (3D) photonic quasicrystals (Penrose with induced deterministic disorder and icosahedral structures)

Optical studies of 1D photonic quasicrystals

To illustrate the importance of the discrete Fourier components, or, equivalently the various RVs of the structure factor in ***k*** space, we analyse the 1D Fibonacci sequence in some detail, and summarize the basic optical properties of 1D quasicrystals that are based on it, using two important examples. First, the transmission spectra from dielectric multilayer stacks composed of two transparent dielectrics of permittivity ε_A and ε_B arranged in a Fibonacci sequence. This is commonly referred to as the 'non-resonant' case[21,25,26] (Fig. 1). Second, the reflectivity and photoluminescence spectra of semiconductor multilayers composed of GaAs QWs embedded between AlGaAs layers of two distinct thicknesses — long and short — where the incident optical frequency is in resonance with both the 2D exciton frequency and the quasicrystal pseudogap[27,28]. This structure is commonly referred to as the 'resonant' case (Fig. 2).

The two approaches to constructing a Fibonacci series involve either substitution[23] or a partial projection from a 2D square lattice[29,30]. In fact, many infinite chains obtained by a substitution rule can be constructed using the projection method[31]; hence the Fibonacci sequence is just one example of many 1D quasicrystals (group 1). The substitution approach to the Fibonacci series starts with a finite sequence of two segments, one long (A, with length L_A) and the other short (B, with length L_B), and operates with the iterative rules $A \rightarrow B$ and $B \rightarrow BA$ for building successive strings of increasing length. If the starting two elements in the sequence are B and A, then the infinite repetition of the operation gives an infinite sequence of A and B that is ordered at long distances. Thus, the structure factor of this series exhibits discrete, sharply defined Fourier components (or RVs). For example, using the iterative rule described above, the sixth member of the Fibonacci series, S_6, results in the sequence *BABBABABBABBA*. If the segment length ratio $L_A/L_B = \tau$ is an irrational number, then the sequence will have no repetitive distance. Interestingly, the ratio of occurrences of A and B in an infinite canonical Fibonacci sequence corresponds to $\tau = 2\cos(36°) = (1 + \sqrt{5})/2 \approx 1.618034$, the so-called 'golden ratio'[32,33].

The complete approach to the Fourier transform analysis of a Fibonacci chain was first presented by Levine and Steinhardt[20], and later expanded by several other researchers[34,35]. The Fibonacci structure factor consists of a set of discrete Fourier components (which may produce sharp diffraction Bragg peaks) that densely fill the ***k*** space. For an infinite Fibonacci set, the discrete Fourier components occur at $Q_{hh'}$, which can be calculated from two independent integers, h and h':

$$Q_{hh'} = \frac{2\pi}{L_B}\frac{\tau^2}{\tau^2+1}\left(h + \frac{h'}{\tau}\right),$$

where $L_B\ (\tau^2 + 1)/\tau^2 = L_B\ (3 - \tau) = d$, the 'mean period'. Here, $d = (N_AL_A + N_BL_B)/(N_A + N_B)$, where N_A and N_B are the number of segments of A and B, respectively. The Fourier components $f_{hh'}$ associated with $Q_{hh'}$ can be rigorously calculated[23]. The largest $|f_{hh'}|$ values correspond to the integers h and h' that are successive Fibonacci numbers: that is, $(h, h') = (F_j, F_{j-1})$. The Fibonacci numbers F_j are given by the recursion rule $F_j = F_{j-1} + F_{j-2}$, starting with $F_1 = F_2 = 1$. The largest initial $f_{hh'}$ are therefore f_{11} and f_{21}, where both f values are ~1; f_{10} and f_{01} are much smaller (~0.1), and other $f_{hh'}$ are even smaller (~0.01) (Fig. 1c).

Non-resonant Fibonacci quasicrystals. We begin by considering the pioneering non-resonant Fibonacci quasicrystals that initiated the study of quasicrystalline order in optics. Such structures are constructed from two dielectric slabs (or layers) of permittivity ε_A and ε_B ($\varepsilon_A \neq \varepsilon_B$) with thicknesses of L_A and L_B, respectively (Fig. 1a)[25,26,36–38]. The role of the structure factor in this case is played by the Fourier components ε_G of the dielectric constant $\varepsilon(z)$, such that $\varepsilon(z) = \sum_G \varepsilon_G \exp(iG \cdot z)$, where $G = \pm Q_{hh'}$. The components ε_G have been calculated rigorously and shown to scale with $f_{hh'}$ (ref. 39). It was shown

that the electric field $E(z)$ of light propagating in the multilayered structure satisfies the 1D wave equation[40]

$$\left[-\frac{d^2}{dz^2} - q^2\right] E(z) = 2q\sum_G \exp(\mathrm{i}G \cdot z) P_G E(z)\,, \qquad (1)$$

where $q = \omega c/\sqrt{\varepsilon}$, $P_G = q\varepsilon_G/2\varepsilon$ and ε is the average dielectric constant given by the relation $\varepsilon = (\varepsilon_A N_A L_A + \varepsilon_B N_B L_B)/(N_A L_A + N_B L_B)$, which is equivalent to $\varepsilon = (\varepsilon_A(\tau + 1) + \varepsilon_B)/(\tau + 2)$. Using equation (1), it is possible to write the electromagnetic field $E(z)$ in the aperiodic structure as a superposition of 'Bloch-like' waves, $E_K(z) = \sum_G \exp(i(K-G)\cdot z)\, E_{K-G}$, which can be calculated numerically using the coefficients ε_G of the Fibonacci sequence[28]. Using this method, the reflectivity and transmission spectra can be readily calculated (Fig. 1b); this was the first optical demonstration of the behaviour of quasicrystalline order[25]. It is apparent that the spectra contain many forbidden gaps at photon energies $\omega_{hh'} = (c/\sqrt{\varepsilon})G/2$; that is, at the edges of the 'quasi-Brillouin zone' that corresponds to the reciprocal vectors $\mathbf{k} = G/2$ (and $G = Q_{hh'}$), having widths that are proportional to P_G (which in turn is proportional to the Fourier components $f_{hh'}$).

Another approach for calculating the transmission spectrum of a Fibonacci quasicrystal is the beautiful 'trace map' method introduced by Kohmoto *et al.* in 1987[21] and further developed by Wang *et al.* in 2000[41]. These researchers calculated the optical transmission through Fibonacci multilayers using the transfer matrix M, based on light propagation through layers A (matrix T_A), B (matrix T_B), and across the interfaces A → B and B → A (matrices T_{AB} and T_{BA}, respectively). The transfer matrix of multilayers based on the first two Fibonacci elements are $M_1 = T_A$ and $M_2 = T_{AB}T_BT_{BA}T_A$. M_j for higher Fibonacci numbers are calculated using the recursion relation $M_j = M_{j-2}M_{j-1}$. This is the same as the renormalization-group equation for a quasiperiodic Schrödinger equation and has been studied extensively. It can be considered as a dynamical map of M_j trace, X_j (hence its name), and was shown to possess a constant of motion for X_j. In this approach, the transmission spectrum T is calculated using the relation $T = 4/(M_j^2 + 2)$, where M_j^2 is the sum of the squares of the four elements of M_j. The transmission spectra based on this approach were shown to fit experimental results accurately[25]. The beauty of this approach is that it establishes a far-reaching correspondence between 1D optics in quasicrystals and dynamical systems theory.

To demonstrate the optical transmission properties of a 1D Fibonacci structure, Fig. 1b shows the optical transmission spectra of S_n structures that contain finite numbers, F_6, F_7 and F_8 (having 13, 21 and 34 layers, respectively) stacked films of SiO_2 (A; $n_A = 1.45$) and TiO_2 (B; $n_B = 2.30$), where n is the refractive index, arranged in the Fibonacci sequence[25]. The structures were designed such that $n_AL_A = n_BL_B$. It is clear that the positions of minima in the transmission spectrum (Fig. 1b, top panels) are well-correlated with the optical gaps (or 'pseudo gaps') obtained in the nine-wave calculation (Fig. 1c, bottom panels) using the Bloch-like Fourier component method, which opens at $\mathbf{k} = G/2$ and $G = Q_{hh'}$. In addition, the largest pseudo-gaps correspond to the largest $f_{hh'}$ for $hh' = 1, 1$ (for Fibonacci numbers F_0, F_1) and 1, 2 (F_1, F_2), respectively. Note also the self-similarity of the transmission spectrum, which is one of the most important characteristics of optical spectra based on quasicrystals[21]. In fact, Gellerman *et al.*[25] explicitly showed that the four multilayers having the Fibonacci sequences S_5 and S_6, and S_8 and S_9 have similar transmission spectra when the frequency axis is multiplied by an appropriate scaling factor. Measurements of the phase change of light incident on a Fibonacci structure[26] revealed that the self-similarity of the Fibonacci optical spectrum dominates the phase change and transmission spectra.

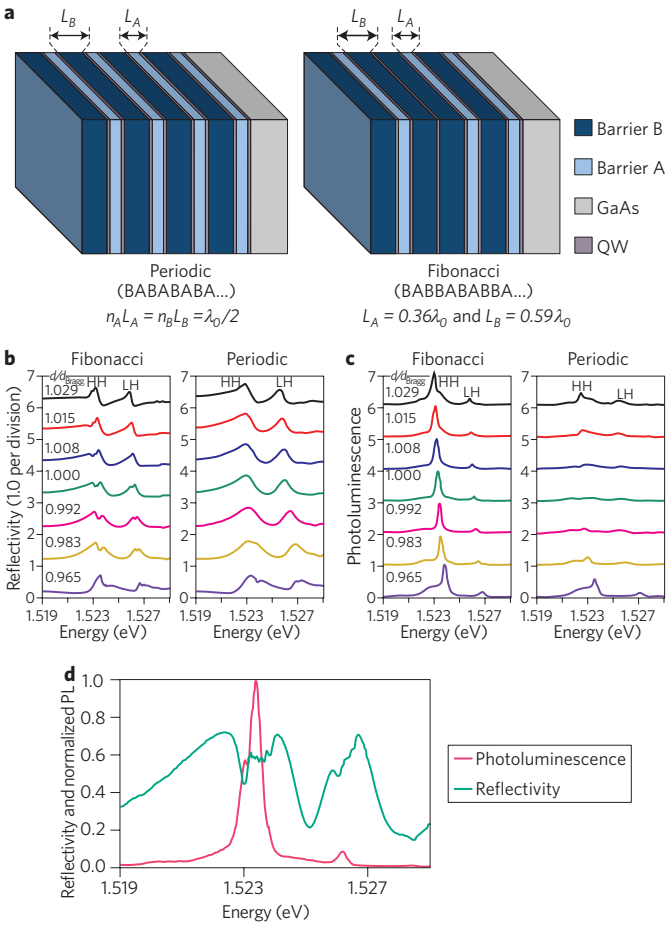

Figure 2 | Resonant 1D Fibonacci quasicrystalline structure. a, Schematic of a Fibonacci structure containing GaAs QWs sandwiched between the short (A) and long (B) AlGaAs barrier layers. **b**, Comparison of the thickness dependence of the reflectivity of both Fibonacci (i) and periodic (ii) multilayers. The spacing of the 21 QWs is a Fibonacci sequence with optical thicknesses (at the Bragg condition) of $A = 0.36\lambda_0$ and $B = 0.59\lambda_0$ (ii) or equidistant at $\lambda_0/2$ (i). A reflectivity dip is present at the Bragg resonance only in (ii), which indicates larger absorption inside the stop band. Each curve of larger d/d_{Bragg} is shifted up by one unit of reflectivity from the preceding one. **c**, Comparison of photoluminescence intensities from Fibonacci (i) and periodic (ii) multilayers. Conditions are the same as in **b**, with weak excitation at 1.59 eV. The photoluminescence from light-hole excitons is weak because of their rapid relaxation. The photoluminescence is strong at the Bragg condition only in the Fibonacci case (i). Equal vertical shifts separate the spectra of different d/d_{Bragg}. **d**, Photoluminescence and reflectivity of QW Fibonacci chain. The optical thicknesses (at Bragg condition) are $A = 0.36\lambda_0$ and $B = 0.59\lambda_0$; $N = 54$. The photoluminescence, heavy-hole (HH) and light-hole (LH) peaks coincide with the dips in reflectivity. Figure **b**–**d** reproduced with permission from ref. 27, © 2008 OSA.

The self-similarity property of quasicrystal transmission spectra raises the question of whether the photon wavefunction at frequencies inside the pseudo-gaps is localized or extended. It turns out that it is neither. In fact, the photon wavefunction decays exponentially outside the pseudo-gaps, but shows critical behaviour (or critical states) of a multifractal nature inside the pseudo-gaps, which does not decay completely even at long distances[42–45]. The fascinating properties of the critical states in quasicrystals and their role in transport[44–46] are the subject of a myriad of research papers (an excellent review can be found in ref. 18).

NATURE PHOTONICS DOI: 10.1038/NPHOTON.2012.343

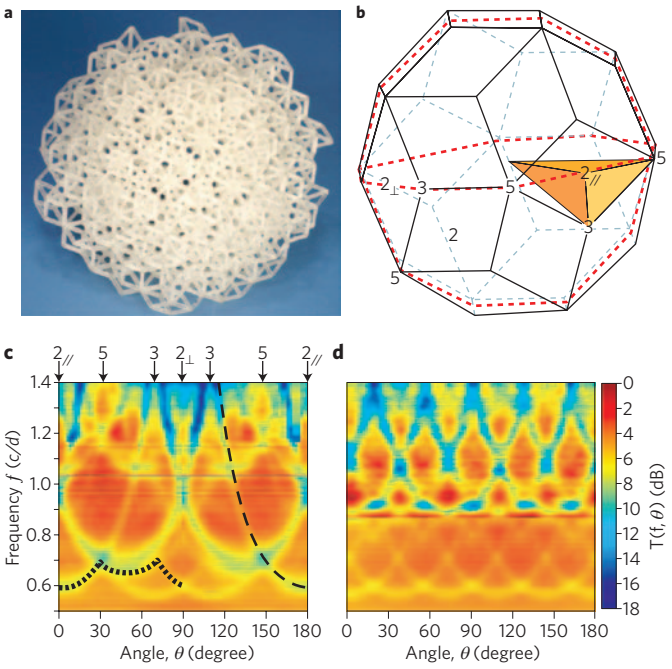

Figure 3 | 3D photonic quasicrystal and its transmission properties. **a**, 3D icosahedral quasicrystal with 1-cm-long rods fabricated by stereolithography. **b**, Triacontahedron, one of several possible effective Brillouin zones (related to the pseudo-Jones zone used in describing electronic transport in quasicrystals) with icosahedral symmetry. The irreducible Brillouin zone is highlighted in yellow. **c**, Transmission $T(f, \theta)$ as a function of frequency (f, measured in units of c/d) and angle (θ) for a rotation about a two-fold rotation axis of the quasicrystal (corresponding to the dotted line in **b**) using two overlapping frequency bands. The dashed line is a $1/\cos\theta$ curve characteristic of Bragg scattering from a Brillouin zone face. **d**, $T(f, \theta)$ for a rotation about a five-fold rotation axis that corresponds to the dashed line in **b**. Figure **a**–**d** reproduced with permission from ref. 63, © 2005 NPG.

Resonant Fibonacci quasicrystals

To describe resonant quasicrystal optics, we start with regular photonic crystals. Periodic structures in which the dielectric response contains an excitonic resonance at frequency ω_0 are known as resonant photonic crystals[47]. Electromagnetic waves at frequencies close to the resonance form exciton–polaritons, which are hybrid quasi-excitations of photons and excitons[48,49]. Similarly, it is possible to define resonant photonic quasicrystals and other aperiodic deterministic sequences. Sivachenko *et al.*[49] (theory) and Eradat *et al.*[50] (experiment) were the first to study exciton–polaritons in resonance with the stop-band in opal photonic crystals (periodic structures) infiltrated with cyanine dye aggregates, which are highly polarizable media with very large Rabi frequencies. They used the angle-dependent tunability of the stop-band in opal photonic crystals along the [111] direction to investigate the reflectivity at resonance with the dye exciton polaritons[50]. At the resonance condition, they showed that the Bragg stop-band decomposes into two reflectivity bands with a semitransparent spectral range in between, due to the propagation of 'Braggoriton' excitations — hybrid quasiparticles of photons and excitons subjected to the Bragg diffraction condition — inside the gap[49,50].

Poddubny *et al.*[32] were the first to advance the idea of resonant photonic quasicrystals. They proposed a multi-QW structure, in which the exciton frequency ω_0 was tuned to the 1D photonic band-gap of the stack. As noted above, the largest values of the Fourier components $f_{hh'}$ for photonic quasicrystals based on the Fibonacci sequence are reached for integer hh' pairs that are two successive Fibonacci numbers, F_mF_{m-1}. Under these conditions, the Fibonacci structures are resonant and strongly coupled when the exciton at frequency ω_0 coincides with an energy pseudo-gap at $Q_{hh'}$, formed from hh' pairs (for example, Q_{11}). In such cases, the photoluminescence of the stack may exhibit 'super-radiance' behaviour, whereby the emission lifetime is shorter and the emission intensity is stronger than that in non-resonant conditions. In addition, the wave equation (equation (1)) in such structures contains a resonant polarization term due to the exciton–polariton: namely $P_G = \mu f^*_{hh'}$ and $P_{-G} = \mu f_{hh'}$, where $\mu = (L_B)^{-1}(1/\tau^2 + 1)F(\omega - \omega_0)$ and $F(\omega - \omega_0)$ is the resonant term[28]. This leads to the appearance of an allowed mini-band inside the forbidden 1D pseudo-gap. Therefore, resonant Fibonacci multi-QW stacks show both high photoluminescence emission intensity[51] and optical modulation features in their reflectivity spectrum, which do not exist in multi-QW stacks based on periodic structures (Fig. 2b,c)[27].

Experimental verification of this model was performed by Hendrickson *et al.*[27] and Werchner *et al.*[28] using canonical (where $L_B/L_A = \tau$, the golden ratio) and non-canonical ($L_B/L_A \neq \tau$) Fibonacci sequences, respectively. The multi-QW stacks were made of GaAs QWs sandwiched between long and short AlGaAs barrier layers, arranged in a Fibonacci sequence. The Bragg condition for the canonical Fibonacci structure can be presented in the same form as for the periodic structure, namely $d = d_{\mathrm{Bragg}}$, where d is the 'mean period' of the structure ($d = (3 - \tau)L_B$), $d_{\mathrm{Bragg}} = \lambda_0/2n_{\mathrm{eff}}$ for the exciton, and n_{eff} is the effective refractive index of the QW. Figure 2b,c compares the reflectivity and photoluminescence emission spectra of two multilayer structures having periodic- and Fibonacci-type order[27]. In the periodic case, the resonance condition lifts the N-fold degeneracy, where N is the number of layers in the stack, so that one mode becomes super-radiant whereas the other $N-1$ modes are subradiant[51]. However, the super-radiant mode for perpendicular emission has nodes at the QW in each layer that lead to inefficient emission intensity. This behaviour can be explained by employing a frequency-domain analysis, where the resonant emission frequency falls in the stop-band of the underlying 1D photonic crystal. This condition, however, does not occur for the Fibonacci QW structure, as there is the possibility of photoluminescence emission inside the pseudo-gap due to the strong coupling that occurs in the 1D quasicrystal that leads to the existence of states in the forbidden gap. As seen clearly in Fig. 2b, when the structure is in resonance, the reflectivity shows typical spectral features inside the quasi-gap that do not exist in the gap of the periodic structure. In contrast, the photoluminescence emission in the Fibonacci structure remains strong compared with that in the periodic structure (Fig. 2c).

Photonic quasicrystals in higher dimensions

Higher-dimensional photonic quasicrystals (2D and 3D) offer greater flexibility over 1D structures in the design of their geometry and potential applications. For example, several 1D quasicrystals, such as the Fibonacci sequence structure, can be extended to 2D[52–54]. However, the design rules become increasingly complex as one considers the broader range of deterministic aperiodic structures. This is demonstrated by the fact that tiling rules for 2D quasicrystals do not exist for geometries that exhibit more than 14-fold rotational symmetry[17]. Along with the increase in geometrical complexity, there is a corresponding increase in the complexity of the mathematical description of the properties of electromagnetic propagation. Even without a detailed analytical description, however, good physical insight into the propagation properties of light can be still obtained in various photonic quasicrystals.

One of the most common 2D quasicrystals was discovered by Roger Penrose. This structure utilizes two different types of tiles to

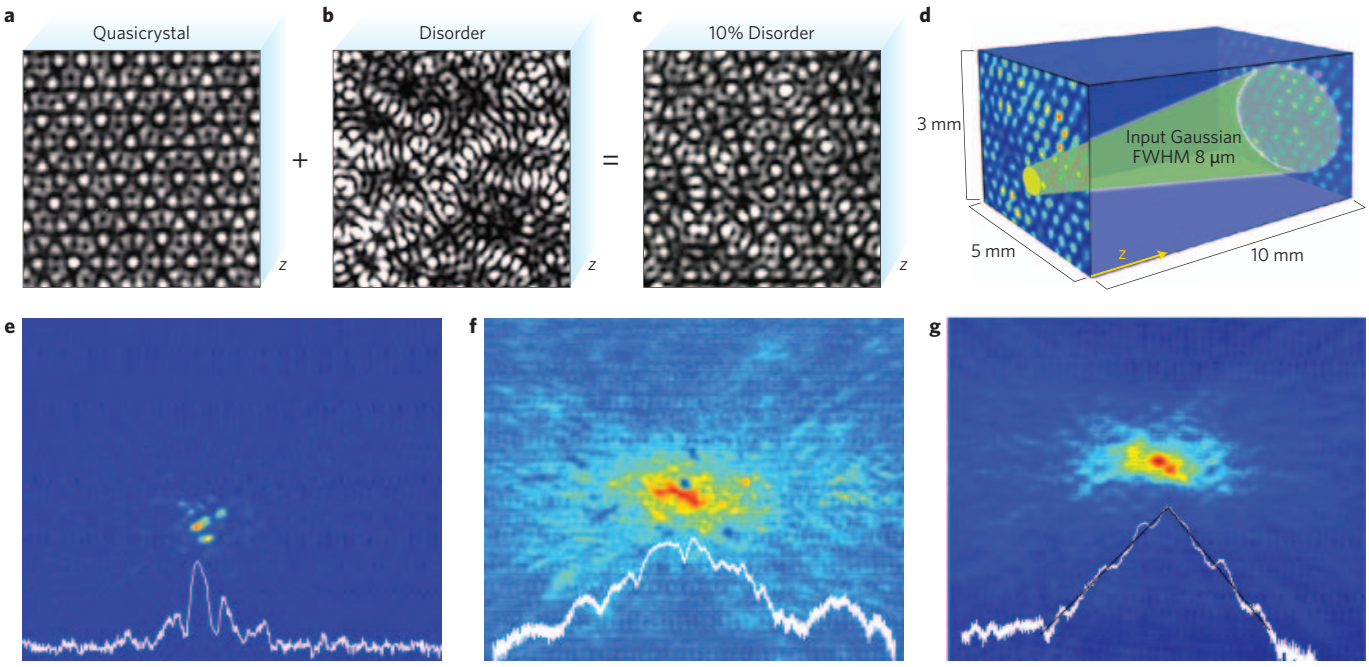

Figure 4 | Disorder-enhanced transport and localization in 2D photonic quasicrystals. a–c, Light incident at the input face of a 2D quasicrystal lattice without (**a**) and with (**b**,**c**) disorder. **d**, For various degrees of disorder, the output intensity pattern is monitored and ensemble-averaged. **e**, When no disorder is present, the probe beam width increases in the *z* direction, which demonstrates some light transport in the perpendicular *x*–*y* plane, but with an intermittent intensity pattern at the output plane. **f**, At 10% disorder, the structure still resembles a Penrose structure but with a dramatic increase in probe beam width, which demonstrates increased transport in the *x*–*y* plane. **g**, When the disorder is increased to 50%, the structure looks almost random and the output beam becomes gradually more localized. Figure reproduced with permission from ref. 46, © 2011 AAAS.

fill all of the 2D space: a thin rhomb, with vertex angles of 36° and 144°, and a fat rhomb, with vertex angles of 72° and 108° (ref. 55). The pattern exhibits local five-fold symmetry in real space, whereas the structure factor exhibits ten-fold rotational symmetry and consists of a series of discrete spots surrounding the central 'undiffracted' spot. In contrast with periodic crystals, for which the reciprocal lattice can be defined in terms of a set of primitive RVs, the RVs associated with quasicrystals densely fill the reciprocal space so that no primitive set of RVs can be defined. Nevertheless, a set of relatively intense RVs can be chosen to describe the structure. In the case of Penrose tiling, a basic set can be defined using five RVs, denoted by $\pm F^{(i)} = \cos((i-1)\pi/5)$, $\sin((i-1)\pi/5)$ in Cartesian coordinates for $i = 1\ldots5$ (refs 56,57). The magnitude of each $F^{(i)}$ is related to the tile side length d through the relation $|F^{(i)}| = 2\pi/(d\cos(\pi/10))$. Analogous to the canonical Fibonacci series, the ratios of the different RVs are related to the golden ratio, $\tau = 1.618$. Using the Penrose structure among others, we describe below examples of light propagation and laser action in which the RVs play a major role in determining the optical properties.

The photon dispersion relations inside periodic photonic crystals (having Bravais lattices) are periodic in reciprocal space. Therefore, the photonic band structure is essentially defined by the dispersion properties in the first Brillouin zone. Quasicrystals, however, do not exhibit a strict Brillouin zone. Nevertheless, it is still possible to construct an 'effective Brillouin zone' by defining a decagon in reciprocal space that is formed from the lines bisecting the basic set of RVs, $F^{(i)}$, which is referred to as the 'pseudo-Jones' zone[23]. The photonic dispersion relations in this region govern the basic properties of light propagation. In periodic photonic crystals, a complete photonic bandgap arises when the spectral gaps at the Brillouin zone boundaries overlap in all directions. The anisotropy of the bandgap is dependent on the symmetry of the underlying photonic crystal lattice. In photonic quasicrystals, as the rotational symmetry of the pseudo-Jones zone increases, the bandgap becomes more circular in 2D (or spherical in 3D), which can result in a complete bandgap[56–60]. The trade-off between the weaker scattering that exists in photonic quasicrystals due to the small $f_{hh'}$ compared with that in periodic photonic crystals, together with the increased isotropy in photonic quasicrystals, was recently discussed by Steinhardt and co-workers[61]. They concluded that photonic quasicrystals have a better chance of showing a complete gap for a low dielectric contrast between the dielectric constituents; however, for high dielectric contrast the resulting increase in light scattering overcomes the need for isotropy, and thus periodic photonic crystals are better. Also, we note that in periodic 2D photonic crystals, the highest level of rotational symmetry is six; 2D photonic quasicrystals, in contrast, offer the potential for much higher rotational symmetry, where symmetries of 10 (Penrose) and 12 (dodecahedron) are common[24].

Fabrication techniques for photonic quasicrystals

It is instructive to discuss the various fabrication techniques that have been developed for creating 2D and 3D photonic quasicrystals. The most common approaches involve direct laser writing[62–64] or interference between multiple laser beams[46,65–70]. These procedures can be accomplished in many material systems, including one-[63–67] or two-photon[68] curing of ultraviolet-sensitive polymers, or the use of photorefractive crystals[69,70]. An alternative to these approaches involves direct lithographic reproduction of a quasiperiodic pattern[71]. For example, Zoorob *et al.*[58] fabricated cylindrical air rods in a 12-fold rotationally symmetric pattern to create a 260-nm-thick silicon-nitride-based waveguide. The structure possessed several characteristics that clearly differentiate it from a periodic lattice, the most noteworthy being the ability to create a bandgap even when using low-refractive-index materials such as glass ($n = 1.45$). In contrast with periodic crystals, where the

NATURE PHOTONICS DOI: 10.1038/NPHOTON.2012.343

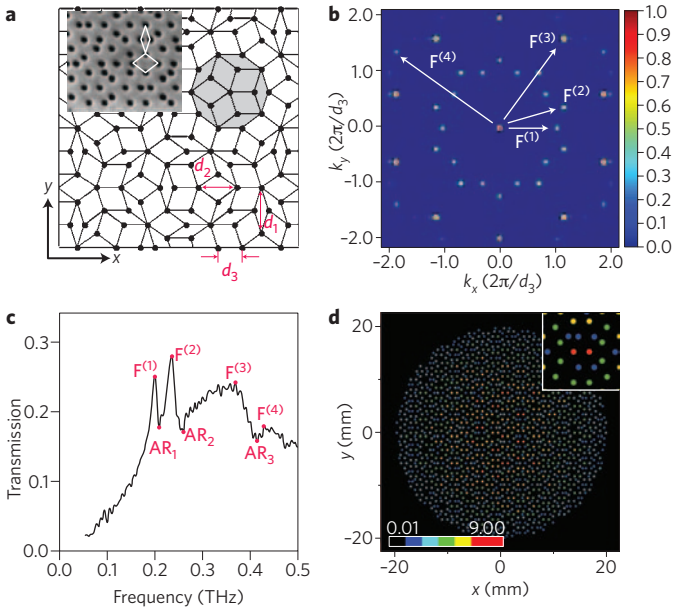

Figure 5 | Transmission properties of SPP-based quasiperiodic plasmonic hole arrays. a, Real-space representation of a 2D Penrose-type quasicrystal hole array constructed of fat and thin rhomb tiles on a 75-μm-thick free-standing stainless-steel film with apertures fabricated at the vertices; d_3 corresponds to the length of the rhomb side. **b**, Reciprocal-space representation of the 2D aperture array shown in **a**. The ten-fold rotational symmetry is apparent from the reciprocal vectors, given by $F^{(i)}$ in the Fourier space representation. **c**, Electric field transmission spectrum $T(\nu)$ of a Penrose quasicrystal hole array with d_3 = 1.5 mm and aperture diameter D = 540 μm. The resonance bands $F^{(i)}$ in the spectrum correspond to the RVs in the structure factor representation of the Penrose structure in **b**. The anti-resonance (AR) features are assigned and correspond to dips in $T(\nu)$ that occur at the high-frequency side of each resonant band. **d**, Per-hole transmission (normalized to the single-hole transmission) through the Penrose hole array structure at λ = 0.98 mm. Figure reproduced with permission from: **a**,**b**, ref. 24, © 2007 NPG; **a** (inset), ref. 122, © 2009 Elsevier; **c**, ref. 82, © 2007 OSA; **d**, ref. 83, © 2007 APS.

inclusion of a defect produces one fixed set of localized defect modes, a single defect in a photonic quasicrystal can produce different localized states that depend on the specific location in the pattern, owing to differences in the local dielectric environment that result from the lack of translational symmetry[59].

Three-dimensional photonic quasicrystals were first experimentally demonstrated by Man *et al.*[63], who used stereolithography to create an icosahedral structure via ultraviolet photopolymerization (Fig. 3). The quasicrystal had 12 five-fold, 15 three-fold and 30 two-fold symmetry axes. Using microwave transmission measurements, about a two-fold rotation axis and a five-fold rotation axis, they found a relatively well-defined effective Brillouin zone, despite the increased density of discrete spots in reciprocal space. They also found that the effective Brillouin zone was nearly spherical, with only a small difference (~17%) in the pseudo-gap centre. However, they were unable to find a complete bandgap; in fact, the question of whether a complete photonic gap may exist in photonic quasicrystals is still unresolved.

Light propagation in 2D photonic quasicrystals

It is instructive to examine the role of disorder in photon localization in two-dimensional quasicrystals. As disorder is introduced into a photonic crystal, the nature of light propagation through the material changes from ballistic to diffusive. With increasing disorder, the interference between individual scattering events ultimately causes the light to become spatially localized — an effect known as Anderson localization. In contrast with this behaviour, it has been suggested that disorder in photonic quasicrystals can actually enhance transport prior to localization. To understand this seemingly counterintuitive property, Levi *et al.*[46] used a technique known as optical induction[71,72] to prepare a 2D Penrose pattern in a photorefractive crystal. The diffraction pattern created by the interfering pump beams yielded a rewritable refractive index pattern that allowed for the introduction of disorder by using diffusers in the pump beam path. The resulting quasicrystal pattern constrained light only in the x–y plane, thus allowing for free propagation along the z axis. It was shown[46] that the transverse optical properties are governed by the paraxial equation

$$i\frac{d\Psi}{dz} = \left[-\frac{1}{2k}\left(\frac{\partial^2}{\partial x^2}+\frac{\partial^2}{\partial y^2}\right) - \frac{k}{n_o}\Delta n(x,y)\right]\Psi \qquad (2)$$

where Ψ is the slowly varying envelope of the optical field, z is the propagation axis, $k = \omega n/c$ is the propagation constant, n_0 is the bulk refractive index and Δn is the local change in the refractive index. Equation (2) has the form of Schrödinger's equation if the substitutions $z \rightarrow t$ (time) and $\Delta n \rightarrow V$ (potential) are made. Propagation through this type of medium is therefore equivalent to observing the temporal variation of the wave packet as it propagates in time. In the absence of any transverse disorder, Levi *et al.* observed an intermittent intensity pattern resembling a broadened version of the Penrose geometry at the output plane (Fig. 4). As the introduced disorder increased to 10%, the intensity pattern broadened spatially, corresponding to enhanced transport in the x–y plane, thus verifying earlier predictions[73]. However, as the introduced disorder was further increased, light propagation transformed from ballistic to diffusive, followed by inevitable Anderson localization. This approach therefore offers a unique means for the real-time observation of disorder-enhanced light transport in photonic quasicrystals in a controllable manner.

Plasmonics in metallic photonic quasicrystals

Whereas most of the optical techniques discussed so far utilize photonic quasicrystals made from dielectric media (both insulators and semiconductors), recently there has been interest in utilizing collective charge oscillations along metal–dielectric interfaces — surface plasmon–polaritons (SPPs) — for the subwavelength control and manipulation of light[74]. By utilizing stationary localized surface plasmons in metal nanoparticles, or propagating SPPs along metal–dielectric interfaces, unprecedented control over light–matter interactions has been achieved[75–77]. Such interactions have led to significant advances in the ability to obtain large field enhancements, as well as the localization and modification of the local density of states. The plasmon mediated in- and out-coupling of incident light, which governs both the near- and far-field optical properties of these structures, strongly depends on the shape and size of individual features, as well as the structure factor of the underlying array. In the case of periodic arrays with pitch p, the spectral resonances can be conveniently described by an underlying Bravais lattice that has basic primitive vectors based on $G^{(i)} = 2\pi/p$, and studied using well-established analytical tools that include the Brillouin zone and the Bloch theorem. In contrast, even though aperiodic arrays exhibit significantly richer optical spectra, light–matter interactions in such structures are not as well understood and require the development of sophisticated measurement techniques and numerical tools.

As an example, in Fig. 5 we summarize the SPP-mediated enhanced optical transmission properties of aperture arrays fabricated in a 2D Penrose-type quasicrystal geometry. Analogous to periodic arrays, the coupling of incident light to SPPs in these

structures can be explained by using a quasi-momentum conservation rule[24]: $\mathbf{k}_{||} + \mathbf{k}_{SPP} = F^{(i)}$, where $\mathbf{k}_{||}$ is the in-plane wave vector of the incident light, $\mathbf{k}_{SPP}$ is the SPP wave vector and $F^{(i)}$ correspond to the discrete Fourier transform vectors in the structure factor (RVs). Figure 5b shows the corresponding geometrical structure factor associated with the Penrose-type lattice. As noted above, $|F^{(i)}|$ can be directly associated with real-space distances d_i in the quasicrystal structure. The RVs were shown to be related to a series of Fano-type resonances observed in the transmission spectra, $T(\nu)$, through the 2D structure (Fig. 5c), where the resonances occur at frequencies $\nu_i \approx c|F^{(i)}|$. It was deduced that the resulting spectral features in $T(\nu)$ are a consequence of Fano-type interference between discrete transmission lines associated with the structure factor, and a transmission continuum that results from the optical properties of individual apertures[24].

The enhanced transmission studies using Penrose quasicrystal structures shown here in the terahertz frequency range have since been extended to other regions of the electromagnetic spectrum[78–81], as well as to other quasicrystal geometries such as octagonal and dodecagonal 2D quasicrystals[79,82] and 'approximate' quasicrystal structures designed using an inverse Fourier transform algorithm to exhibit arbitrary n-fold rotational symmetries[24,82]. The SPP-mediated Fano resonances in the transmission spectrum were explained using an intuitive interference model in which SPPs launched by the scattering of incident light from individual features accrue a phase shift and interfere constructively or destructively based on the design of the underlying array, thereby allowing the spectral shape of the optical response to be determined. Sharp spectral peaks can therefore be expected from any plasmonic array — periodic or aperiodic — that contains discrete RVs in its structure factor, similar to the existence of sharp Bragg diffraction lines in X-ray scattering[23]. In addition to the rich $T(\nu)$ spectra, the per-hole transmission and near-field distribution (Fig. 5d) in these structures have been theoretically shown to vary spatially and exhibit localized hot spots with rotational symmetries that are unique to quasiperiodic structures[83]. Although these studies have helped clarify the physics of light–matter interactions in plasmonic devices and unravel the underlying mechanism that governs the phenomenon of 'enhanced transmission', quasicrystal structures may also enable interesting exotic effects that are not possible with periodic structures. One such example involves the recent demonstration of superfocusing, which may be important for subwavelength imaging or lithography applications[84,85].

Introducing structural aperiodicity in devices that exploit localized surface plasmon resonances associated with arrays of individual metallic nanoparticles can allow arbitrary engineering of the density of spatial frequencies (or, equivalently, the structure factor in the Fourier space) over a broad spectral range[86,87]. As an example, Fig. 6 summarizes the optical scattering properties of a 2D array of nanoparticles arranged in a Fibonacci pattern. The structure factor contains two types of prominent RVs: (i) two sets of four vectors, $\mathbf{G}_1$ and $\mathbf{G}_2$, respectively, where $\mathbf{G}_1 = 2\pi/a(\pm 1{:}0)$ and $2\pi/a(0{:}\pm 1)$, and $\mathbf{G}_2 = 2\pi/a(\pm 1{:}\pm 1)$, which correspond to the underlying grid on which the Fibonacci structure is based; and (ii) three additional sets of eight vectors, $\mathbf{F}_1$ to $\mathbf{F}_3$, which belong to the 2D Fibonacci quasicrystal structure factor. Figure 6c shows the corresponding optical extinction spectra for a 2D Fibonacci array of gold nanoparticles of radii $r = 100$ nm and interparticle separation $a = 50$–500 nm. Similarly, the transmission spectrum through 2D aperture arrays patterned in a 2D Fibonacci hole array structure on free-standing metal films has recently been used to demonstrate weak transmission resonances due to shorter SPP correlation lengths compared with periodic arrays[88]. Using theoretical formulations based on the transfer matrix method, the pseudo-dispersion diagram and photonic density of states of a 1D array of

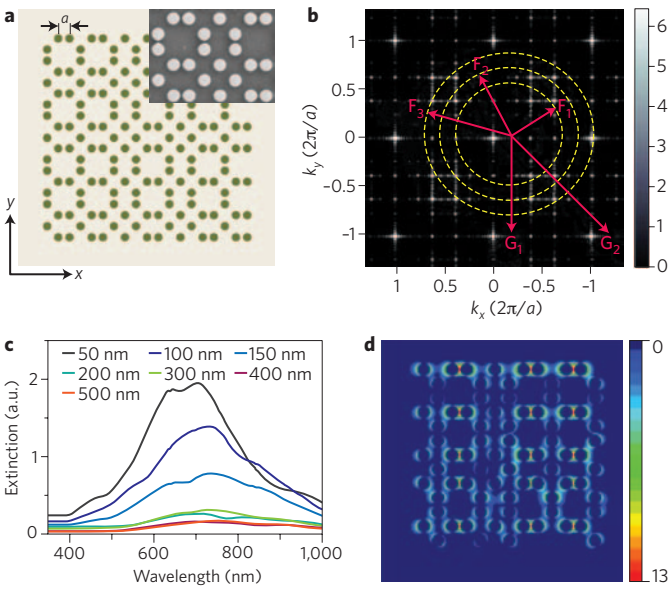

Figure 6 | Optical scattering properties of localized surface plasmon-based quasicrystal plasmonic structures. a, Real-space representation of a generation-7, 2D Fibonacci array, with minimum inter-particle spacing a and radii r. Gold nanoparticles are placed at the location of the dots using electron-beam lithography and subsequent metal deposition. **b**, Reciprocal-space representation of the particle array shown in **a**. **c**, Measured optical extinction spectra for 2D arrays of gold nanoparticles with $r = 100$ nm and a varying from 50 nm to 500 nm. **d**, Calculated electric-field distributions in the plane of the Fibonacci array of gold nanoparticles of $r = 75$ nm and $a = 25$ nm under plane-wave illumination at $\lambda = 785$ nm with the electric field polarization parallel to the x axis. Figure reproduced with permission from: **a**,**b**, ref. 88, © 2012 OSA; **a** (inset),**c**, ref. 94, © 2008 ACS; **d**, ref. 96, © 2009 OSA.

metallic nanoparticles arranged in a Fibonacci pattern was originally calculated by Dal Negro *et al.* to illustrate the existence of plasmonic bandgaps[89]. Subsequent theoretical and experimental works on both 1D and 2D particle arrays have further demonstrated the ability to control and optimize the local field enhancement and localization (Fig. 6d)[90,91], the in-plane optical mode symmetry[92,93], and long-range radiative coupling and scattering[94]. These studies have also resulted in demonstrations of increased sensitivity in biosensing platforms[95], as well as remarkable efficiency improvements in surface-enhanced Raman spectroscopy[96] and photoluminescence[97].

Laser action in aperiodic structures

Laser action requires an optical pump, a gain medium and a feedback mechanism; it can be divided into two classes according to the feedback mechanism involved[98]. The feedback in the first class is provided by mirrors that form a well-defined Fabry–Pérot cavity, whereas the second class is 'mirrorless' and does not require a well-engineered cavity. Mirrorless lasing can be further divided into two categories depending on whether the emission is coherent or incoherent. The first category (coherent emission) includes processes such as super-radiance[99], superfluorescence[100], distributed feedback lasing[101], lasing in photonic crystals[102] and random lasing[103]; whereas amplified spontaneous emission, which is an incoherent phenomenon, belongs to the second category[98]. Aperiodic structures have made important contributions in laser action such as distributed feedback and lasing in photonic quasicrystals, where distributed feedback lasing may be regarded as being part of lasing in 1D photonic crystals. Demonstrations of

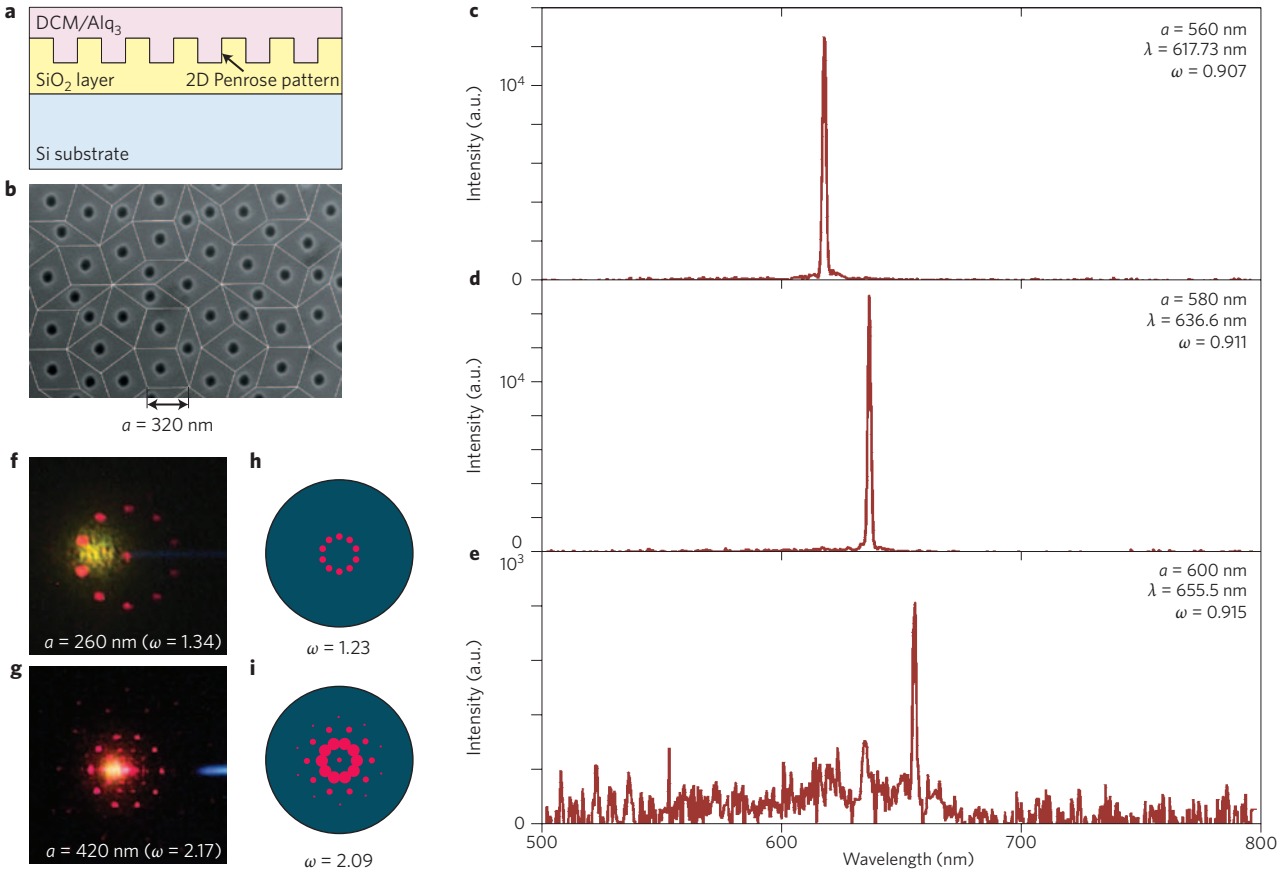

Figure 7 | Lasing action from a 2D photonic quasicrystal. a, Schematic cross-section of a 2D photonic quasicrystal laser. The sample consists of 150-nm-deep quasiperiodic holes patterned in a 1-μm-thick SiO_2 layer on a silicon substrate. The sample was fabricated using electron-beam lithography and reactive ion etching, and finally a 300-nm-thick DCM-doped Alq_3 layer was co-evaporated on the patterned SiO_2. **b**, Scanning electron micrograph of a representative sample, showing the underlying Penrose lattice. **c**–**e**, Emission spectra of samples with minimum inter-aperture distances of 560 nm (**c**), 580 nm (**d**) and 600 nm (**e**), optically pumped using a 0.6 ns pulsed nitrogen laser at 337 nm above the lasing threshold. **f**,**g**, Spot images of the out-of-plane emission measured from samples with quasi-lattice constant a = 260 nm (**f**) and 420 nm (**g**) using a CCD camera. The images show the ten-fold rotational symmetry that is characteristic of the underlying Penrose structure factor. **h**,**i**, Spot images calculated from the RVs in the structure factors for samples with $\omega = 1.23$ (**h**) and 2.09 (**i**), where $\omega = n\lambda/a$ is the normalized lasing frequency. Figure reproduced with permission from ref. 110, © 2004 APS.

lasing in photonic quasicrystals can be divided into two classes — localized and delocalized — according to the characteristic properties of the obtained laser mode.

Lasing in periodic photonic crystals with delocalized laser modes was demonstrated around a decade ago[102,104–106]. The feedback mechanism in this type of laser action is thought to arise from standing-wave solutions to the Bloch wave equations at the photonic band-edges, at points of high symmetry in the Brillouin zone. When the first photonic quasicrystals were fabricated[107–109], researchers realized that photonic 'quasi-bandgaps' can be formed for values of $\mathbf{k}$ in reciprocal space such that $\mathbf{k} = F^{(i)}/2$. It was also understood that the quasi-bandgap width is proportional to the strength of $F^{(i)}$ in reciprocal space. Therefore, the concept underlying photonic crystal lasers can be directly transferred to photonic quasicrystals.

In the pioneering work of Notomi *et al.*[110], the photonic quasicrystal in which lasing was demonstrated was a 2D Penrose structure with ten-fold rotation symmetry in its structure factor (Fig. 7a,b). A Penrose-type hole pattern was fabricated on a SiO_2 substrate superimposed by a laser dye (DCM) embedded in an organic gain medium (Alq_3) (Fig. 7a). If the photonic quasi-bandgap fell within the optical gain spectrum of the lasing medium, then laser action was obtained in the form of a narrow laser mode for sufficiently high excitation intensities (Fig. 7c–e). The researchers found that the laser mode wavelength scaled with the size a of the Penrose pattern (Fig. 7c–e). Surprisingly, the emission pattern obtained was in the form of a number of surface emission laser beams having ten-fold rotational symmetry (Fig. 7f–i). This was taken as evidence that the laser modes in the photonic quasicrystal are extended over the entire structure of at least $100a$, thus showing that the quasicrystal structure is capable of supporting extended optical modes, similar to regular photonic crystals[106]. This is surprising because electronic excitations in quasicrystal materials are thought to be localized, having dispersion relations that contain many mini-gaps[23]. This is apparently not the case for electromagnetic radiation close to the photonic quasicrystal pseudo-gap.

Mahler *et al.*[111] demonstrated lasing in 1D photonic crystals by current injection, rather than optical excitation, in a terahertz quantum-cascade laser based on a 1D Fibonacci distributed feedback sequence. Laser action was obtained in such structures at wavelengths corresponding to band edges at $\mathbf{k} = F^{(i)}/2$ in the structure factor. Unsurprisingly, the mode with the largest Q-factor was found to be associated with $F^{(i)} = Q_{hh'}$ where $h = h' = 1$, as it has the largest Fourier component in the Fibonacci sequence. It was also shown that the laser wavelength scales with the Fibonacci size

parameter. Interestingly, lasing action at multiple wavelengths was obtained when the gain spectrum was broadened. This phenomenon is thought to arise because there are more wave vectors associated with discrete RVs (or $F^{(i)}$) in the Fibonacci sequence than in regular periodic systems, which better matches the extended gain spectrum.

Laser action based on localized modes in photonic quasicrystals has also been demonstrated[112–114]; such laser action has been referred to as 'single-cell cavity mode'. In this case, only a few holes among the 2D quasicrystal hole array were filled with an optical gain medium, thus leading to laser-mode localization. This type of laser action can be thought of as based on a defect mode in which lasing occurs in the optical gap[5,106]. Defect laser action with a very high Q-factor of around 20,000 was predicted[113] for a 2D photonic quasicrystal of dodecagonal structure whose structure factor has 12-fold rotational symmetry, but in reality a Q-factor of only around 1,300 has been achieved so far[114].

Summary

The interesting class of photonic quasicrystals discussed here exhibit unique optical properties because: (i) they can be designed using well-defined algorithms to exhibit controlled interference patterns that lie between those resulting from periodic and random structures; and (ii) they exhibit unique and rich symmetries in Fourier space that are not possible with a periodic lattice. The underlying RVs in reciprocal space show that these aperiodic structures are capable of supporting wave interference. Despite challenges in gaining a fundamental understanding of light–matter interactions in these complex photonic systems, primarily owing to their complexity and a general theory that requires computational models, the initial studies reviewed here have demonstrated that these quasicrystal structures show rich underlying physics and potential technological applications. Because the field of optics has applications across a broad range of areas, the incorporation of controlled structural aperiodicity would allow for unprecedented control over the near- and far-field spectral properties of next-generation photonic devices. Finally, we note that due to space limitations we have not included in this Review several aspects of quasicrystal optics, such as the dynamics of light propagation in 1D photonic quasicrystals[44], nonlinear optics using photonic quasicrystals[115,116], the effect of phasons in the optics of quasicrystals[117,118], and nonlinear light propagation dynamics such as solitons in quasicrystals[119–121]. These interesting subject matters deserve a separate Review.

References

1. Carter, W. H. & Wolf, E. Coherence properties of lambertian and non-lambertian sources. *J. Opt. Soc. Am.* **65,** 1067–1071 (1975).
2. John, S. Strong localization of photons in certain dielectric superlattices. *Phys. Rev. Lett.* **58,** 2486–2489 (1987).
3. Yablonovitch, E. Inhibited spontaneous emission in solid state physics and electronics. *Phys. Rev. Lett.* **58,** 2059–2062 (1987).
4. Joannopoulos, J. D., Meade, R. & Winn, J. *Photonic Crystals: Molding the Glow of Light* (Princeton Univ., 1995).
5. Painter, O. *et al.* Two-dimensional photonic band-gap defect mode laser. *Science* **284,** 1819–1821 (1999).
6. Meier, M. *et al.* Laser action from two-dimensional distributed feedback in photonic crystals. *Appl. Phys. Lett.* **74,** 7–9 (1999).
7. Ebbesen, T. W., Lezec, H., Ghaemi, H., Thio, T. & Wolff, P. Extraordinary optical transmission through sub-wavelength hole arrays. *Nature* **391,** 667–669 (1998).
8. van Albada, M. P. & Lagendijk, A. Observation of weak localization of light in a random medium. *Phys. Rev. Lett.* **55,** 2692–2695 (1985).
9. Wolf, P. E. & Maret, G. Weak localization and coherent backscattering of photons in disordered media. *Phys. Rev. Lett.* **55,** 2696–2699 (1985).
10. Akkermans, E. & Maynard, R. Weak localization of waves. *J. Physique Lett.* **46,** L1045–L1053 (1985).
11. Baleine, E. & Dogariu, A. Variable coherence scattering microscopy. *Phys. Rev. Lett.* **95,** 193904 (2005).
12. Anderson, P. W. Absence of diffusion in certain random lattices. *Phys. Rev.* **109,** 1492–1505 (1958).
13. John, S. Electromagnetic absorption in a disordered medium near a photon mobility edge. *Phys. Rev. Lett.* **53,** 2169–2172 (1984).
14. Cheng, Z., Savit, R. & Merlin, R. Structure and electronic properties of Thue–Morse lattices. *Phys. Rev. B* **37,** 4375–4382 (1988).
15. Liu, N. Propagation of light waves in Thue–Morse dielectric multilayers. *Phys. Rev. B* **55,** 3543–3547 (1997).
16. Dulea, M., Johansson, M. & Riklund, R. Localization of electrons and electromagnetic waves in a deterministic aperiodic system. *Phys. Rev. B* **45,** 105–114 (1992).
17. Steurer, W. & Sutter-Widmer, D. Photonic and phononic quasicrystals. *J. Phys. D* **40,** R229–R247 (2007).
18. Maciá, E. Exploiting aperiodic designs in nanophotonic devices. *Rep. Prog. Phys.* **75,** 036502 (2012).
19. Shechtman, D., Blech, I., Gratias, D. & Cahn, J. W. Metallic phase with long-range orientational order and no translational symmetry. *Phys. Rev. Lett.* **53,** 1951–1953 (1984).
20. Levine, D. & Steinhardt, P. J. Quasicrystals: A new class of ordered structures. *Phys. Rev. Lett.* **53,** 2477–2480 (1984).
21. Kohmoto, M., Sutherland, B. & Iguchi, K. Localization of optics: Quasiperiodic media. *Phys. Rev. Lett.* **58,** 2436–2438 (1987).
22. Albuquerque, E. L. & Cottam, M. G. Theory of elementary excitations in quasiperiodic structures. *Phys. Rep.* **376,** 225–337 (2003).
23. Janot, C. *Quasicrystals: A Primer* 2nd edn (Oxford Univ., 1994).
24. Matsui, T., Agrawal, A., Nahata, A. & Vardeny, Z. V. Transmission resonances through aperiodic arrays of subwavelength apertures. *Nature* **446,** 517–521 (2007).
25. Gellermann, W., Kohmoto, M., Sutherland, B. & Taylor, P. C. Localization of light waves in Fibonacci dielectric multilayers. *Phys. Rev. Lett.* **72,** 633–636 (1994).
26. Hattori, T., Tsurumachi, N., Kawato, S. & Nakatsuka, H. Photonic dispersion relation in a one-dimensional quasicrystal. *Phys. Rev. B* **50,** 4220–4223 (1994).
27. Hendrickson, J. *et al.* Excitonic polaritons in Fibonacci quasicrystals. *Opt. Express* **16,** 15382–15387 (2008).
28. Werchner, M. *et al.* One dimensional resonant Fibonacci quasicrystals: Noncanonical linear and canonical nonlinear effects. *Opt. Express* **17,** 6813–6828 (2009).
29. Valsakumar, M. C. & Kumar, V. Diffraction from a quasi-crystalline chain. *Pramana* **26,** 215–221 (1986).
30. Lin, Z., Kubo, H. & Goda, M. Self-similarity and scaling of wave function for binary quasiperiodic chains associated with quadratic irrationals. *Z. Phy. B* **98,** 111–118 (1995).
31. Bombieri, E. & Taylor, J. E. Which distributions of matter diffract? An initial investigation. *J. Physique* **47,** C3-19–C3-28 (1986).
32. Poddubny, A., Pilozzi, L., Voronov, M. & Ivchenko, E. Resonant Fibonacci quantum well structures in one dimension. *Phys. Rev. B* **77,** 113306 (2008).
33. Lin, Z., Goda, M. & Kubo, H. A family of generalized Fibonacci lattices: self-similarity and scaling of the wavefunction. *J. Phys. A* **28,** 853–866 (1995).
34. Aviram, I. The diffraction spectrum of a general family of linear quasiperiodic arrays. *J. Phys. A* **19,** 3299–3312 (1986).
35. Dharma-Wardana, M. W. C., MacDonald, A. H., Lockwood, D. J., Baribeau, J. M. & Houghton, D. C. Raman scattering in Fibonacci superlattices. *Phys. Rev. Lett.* **58,** 1761–1764 (1987).
36. Peng, R. W. *et al.* Symmetry-induced perfect transmission of light waves in quasiperiodic dielectric multilayers. *Appl. Phys. Lett.* **80,** 3063–3065 (2002).
37. Kaliteevski, M. A., Nikolaev, V. V., Abram, R. A. & Brand, S. Bandgap structure of optical Fibonacci lattices after light diffraction. *Opt. Spectrosc.* **91,** 109–118 (2001).
38. Huang, X. Q., Jiang, S. S., Peng, R. W. & Hu, A. Perfect transmission and self-similar optical transmission spectra in symmetric Fibonacci-class multilayers. *Phys. Rev. B* **63,** 245104 (2001).
39. Sutherland, B. & Kohmoto, M. Resistance of a one-dimensional quasicrystal: Power-law growth. *Phys. Rev. B* **36,** 5877–5886 (1987).
40. Poddubny, A. Wood anomalies in resonant photonic quasicrystals. *Phys. Rev. B* **83,** 075106 (2011).
41. Wang, X., Grimm, U. & Schreiber, M. Trace and antitrace maps for aperiodic sequences: Extensions and applications. *Phys. Rev. B* **62,** 14020–14031 (2000).
42. Maciá, E. Physical nature of critical modes in Fibonacci quasicrystals. *Phys. Rev. B* **60,** 10032–10036 (1999).
43. Fujiwara, T., Kohmoto, M. & Tokihiro, T. Multifractal wave functions on a Fibonacci lattice *Phys. Rev. B* **40,** 7413–7416 (1989).
44. Dal Negro, L. *et al.* Light transport through the band-edge states of Fibonacci quasicrystals. *Phys. Rev. Lett.* **90,** 055501 (2003).
45. Ghulinyan, M. *et al.* Light-pulse propagation in Fibonacci quasicrystals. *Phys. Rev. B* **71,** 094204 (2005).

46. Levi, L. *et al.* Disorder-enhanced transport in photonic quasicrystals. *Science* **332,** 1541–1544 (2011).
47. Ivchenko, E. L. Excitonic polaritons in periodic quantum-well structures. *Sov. Phys. Sol. State* **33,** 1344–1349 (1991).
48. Prineas, J. P. *et al.* Exciton–polariton eigenmodes in light-coupled $In_{0.04}Ga_{0.96}As/GaAs$ semiconductor multiplequantumwell periodic structures. *Phys. Rev. B* **61,** 13863–13872 (2000).
49. Sivachenko, A. Y., Raikh, M. E. & Vardeny, Z. V. Excitations in photonic crystals infiltrated with polarizable media. *Phys. Rev. A* **64,** 013809 (2001).
50. Eradat, N., Sivachenko, A. Y., Raikh, M. E. & Vardeny, Z. V. Evidence for Braggoritons in opal photonic crystals infiltrated with highly polarizable dyes. *Appl. Phys. Lett.* **80,** 3491–3493 (2002).
51. Deych, L., Erementchouk, M., Lisyansky, A., Ivchenko, E. & Voronov, M. Exciton luminescence in one-dimensional resonant photonic crystals: A phenomenological approach. *Phys. Rev. B* **76,** 075350 (2007).
52. Lifshitz, R. The square Fibonacci tiling. *J. Alloy. Compd.* **342,** 186–190 (2002).
53. Fu, X., Liu, Y., Cheng, B. & Zheng, D. Spectral structure of two-dimensional Fibonacci quasilattices. *Phys. Rev. B* **43,** 10808–10814 (1991).
54. Dal Negro, L., Feng, N. & Gopinath, A. Electromagnetic coupling and plasmon localization in deterministic aperiodic arrays. *J. Opt. A* **10,** 064013 (2008).
55. Penrose, R. Pentaplexity: A class of non-periodic tilings of the plane. *Math. Intell.* **2,** 32–37 (1979).
56. Kaliteevski, M. A. *et al.* Two-dimensional Penrose-tiled photonic quasicrystals: From diffraction pattern to band structure. *Nanotechnol.* **11,** 274–280 (2000).
57. Kaliteevski, M. A. *et al.* Diffraction and transmission of light in low-refractive index Penrose-tiled photonic quasicrystals. *J. Phys. A* **13,** 10459–10470 (2001).
58. Zoorob, M. E., Charlton, M. B. D., Parker, G. J., Baumberg, J. J. & Netti, M. C. Complete photonic bandgaps in 12-fold symmetric quasicrystals. *Nature* **404,** 740–743 (2000).
59. Chan, Y. S., Chan, C. T. & Liu, Z. Y. Photonic band gaps in two dimensional photonic quasicrystals. *Phys. Rev. Lett.* **80,** 956–959 (1998).
60. Zhang, X., Zhang, Z. Q. & Chan, C. Absolute photonic band gaps in 12-fold symmetric photonic quasicrystals. *Phys. Rev. B* **63,** 081105 (2001).
61. Rechtsman, M., Jeong, H. C., Chaikin, P., Torquato, S. & Steinhardt, P. Optimized structures for photonic quasicrystals. *Phys. Rev. Lett.* **101,** 073902 (2008).
62. Jurdik, E. *et al.* Quasiperiodic structures via atom-optical nanofabrication. *Phys. Rev. B* **69,** 201102(R) (2004).
63. Man, W., Megens, M., Steinhardt, P. J. & Chaikin, P. M. Experimental measurement of the photonic properties of icosahedral quasicrystals. *Nature* **436,** 993–996 (2005).
64. Ledermann, A. *et al.* Three-dimensional silicon inverse photonic quasicrystals for infrared wavelengths. *Nature Mater.* **5,** 942–945 (2006).
65. Wang, X., Ng, C. Y., Tam, W. Y., Chan, C. T. & Sheng, P. Large-area two-dimensional mesoscale quasi-crystals. *Adv. Mater.* **15,** 1526–1528 (2003).
66. Guo, M., Xu, Z. & Wang, X. Photofabrication of two-dimensional quasi-crystal patterns on UV-curable molecular azo glass films. *Langmuir* **24,** 2740–2745 (2008).
67. Harb, A. *et al.* Holographically formed three-dimensional Penrose-type photonic quasicrystal through a lab-made single diffractive optical element. *Opt. Express* **18,** 20512–20517 (2010).
68. Shir, D. *et al.* Three-dimensional nanostructures formed by single step, two-photon exposures through elastomeric Penrose quasicrystal phase masks. *Nano Lett.* **8,** 2236–2244 (2008).
69. Freedman, B. *et al.* Wave and defect dynamics in nonlinear photonic quasicrystals. *Nature* **440,** 1166–1169 (2006).
70. Freedman, B., Lifshitz, R., Fleischer, J. W. & Segev, M. Phason dynamics in nonlinear photonic quasicrystals. *Nature Mater.* **6,** 776–781 (2007).
71. Fleischer, J. W., Segev, M., Efremidis, N. K. & Christodoulides, D. N. Observation of two-dimensional discrete solitons in optically induced nonlinear photonic lattices. *Nature* **422,** 147–150 (2003).
72. Efremidis, N., Sears, S., Christodoulides, D., Fleischer, J. & Segev, M. Discrete solitons in photorefractive optically induced photonic lattices. *Phys. Rev. E* **66,** 046602 (2002).
73. Mayou, D., Berger, C., Cyrot-Lackmann, F., Klein, T. & Lanco, P. Evidence for unconventional electronic transport in quasicrystals. *Phys. Rev. Lett.* **70,** 3915–3918 (1993).
74. Maier, S. A. *Plasmonics: Fundamentals and Applications* (Springer, 2007).
75. Ozbay, E. Plasmonics: Merging photonics and electronics at nanoscale dimensions. *Science* **311,** 189–193 (2006).
76. Gramotnev, D. K. & Bozhevolnyi, S. I. Plasmonics beyond the diffraction limit. *Nature Photon.* **4,** 83–91 (2010).
77. Schuller, J. A. *et al.* Plasmonics for extreme light concentration and manipulation. *Nature Mater.* **9,** 193–204 (2010).
78. Przybilla, F., Genet, C. & Ebbesen, T. W. Enhanced transmission through Penrose subwavelength hole arrays. *Appl. Phys. Lett.* **89,** 121115 (2006).
79. Pacifici, D., Lezec, H. J., Sweatlock, L. A., Walters, R. J. & Atwater, H. A. Universal optical transmission features in periodic and quasiperiodic hole arrays. *Opt. Express* **16,** 9222–9238 (2008).
80. Papasimakis, N., Fedotov, V. A., Schwanecke, A. S., Zheludev, N. I. & García de Abajo, F. J. Enhanced microwave transmission through quasicrystal hole arrays. *Appl. Phys. Lett.* **91,** 081503 (2007).
81. Hao, R. *et al.* Exotic acoustic transmission through hard plates perforated with quasiperiodic subwavelength apertures. *Europhys. Lett.* **92,** 24006 (2010).
82. Agrawal, A., Matsui, T., Vardeny, Z. V. & Nahata, A. Terahertz transmission properties of quasiperiodic and aperiodic aperture arrays. *J. Opt. Soc. Am. B* **24,** 2545–2555 (2007).
83. Bravo-Abad, J., Fernández-Domínguez, A., García-Vidal, F. & Martín-Moreno, L. Theory of extraordinary transmission of light through quasiperiodic arrays of subwavelength holes. *Phys. Rev. Lett.* **99,** 203905 (2007).
84. Huang, F. M., Chen, Y., García de Abajo, F. J. & Zheludev, N. I. Optical super-resolution through super-oscillations. *J. Opt. A* **9,** S285–S288 (2007).
85. Huang, F. M., Kao, T. S., Fedotov, V. A., Chen, Y. & Zheludev, N. I. Nanohole array as a lens. *Nano Lett.* **8,** 2469–2472 (2008).
86. Zijlstra, P. & Orrit, M. Single metal nanoparticles: Optical detection, spectroscopy and applications. *Rep. Prog. Phys.* **74,** 106401 (2011).
87. Dal Negro, L. & Boriskina, S. V. Deterministic aperiodic nanostructures for photonics and plasmonics applications. *Las. Photon. Rev.* **6,** 178–218 (2012).
88. Nguyen, T. D., Nahata, A. & Vardeny, Z. V. Measurement of surface plasmon correlation length differences using Fibonacci deterministic hole arrays. *Opt. Express* **20,** 15222–15231 (2012).
89. Dal Negro, L. & Feng, N. N. Spectral gaps and mode localization in Fibonacci chains of metal nanoparticles. *Opt. Express* **15,** 14396–14403 (2007).
90. Dong, J. W., Fung, K., Chan, C. & Wang, H. Z. Localization characteristics of two-dimensional quasicrystals consisting of metal nanoparticles. *Phys. Rev. B* **80,** 155118 (2009).
91. Dallapiccola, R., Gopinath, A., Stellacci, F. & Dal Negro, L. Quasi-periodic distribution of plasmon modes in two-dimensional Fibonacci arrays of metal nanoparticles. *Opt. Express* **16,** 5544–5555 (2008).
92. Forestiere, C., Miano, G., Rubinacci, G. & Dal Negro, L. Role of aperiodic order in the spectral, localization, and scaling properties of plasmon modes for the design of nanoparticle arrays. *Phys. Rev. B* **79,** 085404 (2009).
93. Deng, Z. L., Li, Z. H., Dong, J. W. & Wang, H. Z. In-plane plasmonic modes in a quasicrystalline array of metal nanoparticles. *Plasmon.* **6,** 507–514 (2011).
94. Gopinath, A., Boriskina, S. V., Feng, N. N., Reinhard, B. M. & Dal Negro, L. Photonic–plasmonic scattering resonances in deterministic aperiodic structures. *Nano Lett.* **8,** 2423–2431 (2008).
95. Lee, S. Y. *et al.* Spatial and spectral detection of protein monolayers with deterministic aperiodic arrays of metal nanoparticles. *Proc. Natl Acad. Sci. USA* **107,** 12086–12090 (2010).
96. Gopinath, A., Boriskina, S. V., Reinhard, B. M. & Dal Negro, L. Deterministic aperiodic arrays of metal nanoparticles for surface-enhanced Raman scattering (SERS). *Opt. Express* **17,** 3741–3753 (2009).
97. Gopinath, A., Boriskina, S. V., Yerci, S., Li, R. & Dal Negro, L. Enhancement of the 1.54 μm Er^{3+} emission from quasiperiodic plasmonic arrays. *Appl. Phys. Lett.* **96,** 071113 (2010).
98. Siegman, A. E. *Lasers* (Univ. Science Books, 1986).
99. Dicke, R. H. Coherence in spontaneous radiation processes. *Phys. Rev.* **93,** 99–110 (1954).
100. Yariv, A. *Quantum Electronics* (Wiley, 1989).
101. Morthier, G. & Vankwikelberge, P. *Handbook of Distributed Feedback Laser Diodes* (Artech House, 1997).
102. Noda S. *et al.* Polarization mode control of two-dimensional photonic crystal laser by unit cell structure design. *Science* **293,** 1123–1125 (2001).
103. Wiersma, D. The physics and applications of random lasers. *Nature Phys.* **4,** 359–367 (2008).
104. Meier, M. *et al.* Laser action from two-dimensional distributed feedback in photonic crystals. *Appl. Phys. Lett.* **74,** 7–9 (1999).
105. Notomi, M., Suzuki, H. & Tamamura, T. Directional lasing oscillation of two-dimensional organic photonic crystal lasers at several photonic band gaps. *Appl. Phys. Lett.* **78,** 1325–1327 (2001).
106. Shkunov, M. N. *et al.* Tunable, gap-state lasing in switchable directions for opal photonic crystals. *Adv. Func. Mater.* **12,** 21–26 (2002).
107. Chan, Y. S., Chan, C. T. & Liu, Z. Y. Photonic band gaps in two dimensional photonic quasicrystals. *Phys. Rev. Lett.* **80,** 956–959 (1998).
108. Zhang, X., Zhang, Z. Q. & Chan, C. T. Absolute photonic band gaps in 12-fold symmetric photonic quasicrystals. *Phys. Rev. B* **63,** 081105 (2001).
109. Bayindir, M., Cubukcu, E., Bulu, I. & Ozbay, E. Photonic band-gap effect, localization, and waveguiding in the two-dimensional Penrose lattice. *Phys. Rev. B* **63,** 161104 (2001).

110. Notomi, M., Suzuki, H., Tamamura, T. & Edagawa, K. Lasing action due to the two-dimensional quasiperiodicity of photonic quasicrystals with a Penrose lattice. *Phys. Rev. Lett.* **92,** 123906 (2004).
111. Mahler, L. *et al.* Quasi-periodic distributed feedback laser. *Nature Photon.* **4,** 165–169 (2010).
112. Nozaki, K. & Baba, T. Quasiperiodic photonic crystal microcavity lasers. *Appl. Phys. Lett.* **84,** 4875–4877 (2004).
113. Kim, S.-K. *et al.* Photonic quasicrystal single-cell cavity mode. *Appl. Phys. Lett.* **86,** 031101 (2005).
114. Nozaki, K. & Baba, T. Lasing characteristics of 12-fold symmetric quasi-periodic photonic crystal slab nanolasers. *Jpn J. Appl. Phys.* **45,** 6087–6090 (2006).
115. Lifshitz, R., Arie, A. & Bahabad, A. Photonic quasicrystals for nonlinear optical frequency conversion. *Phys. Rev. Lett.* **95,** 133901 (2005).
116. Bratfalean, R. T., Peacock, A. C., Broderick, N. G. R., Gallo, K. & Lewen, R. Harmonic generation in a two-dimensional nonlinear quasi-crystal. *Opt. Lett.* **30,** 424–426 (2005).
117. De Boissieu, M. Phason modes in quasicrystals. *Phil. Mag.* **88,** 2295–2309 (2008).
118. Widom, M. Discussion of phasons in quasicrystals and their dynamics. *Phil. Mag.* **88,** 2339–2350 (2008).
119. Clausen, C. A. B., Kivshar, Y. S., Bang, O. & Christiansen, P. L. Quasiperiodic envelope solitons. *Phys. Rev. Lett.* **83,** 4740–4743 (1999).
120. Lederer, F. *et al.* Discrete solitons in optics. *Phys. Rep.* **463,** 1–126 (2008).
121. Chen, Z., Segev, M. & Christodoulides, D. N. Optical spatial solitons: Historical overview and recent advances. *Rep. Prog. Phys.* **75,** 086401 (2012).
122. Xue, J. *et al.* Surface plasmon enhanced transmission through planar gold quasicrystals fabricated by focused ion beam technique. *Microelectron. Eng.* **86,** 1131–1133 (2009).

Acknowledgements

This work was supported by the NSF-MRSEC programme at the University of Utah, grant No. DMR 11-21252.

Additional information

Reprints and permissions information is available online at www.nature.com/reprints. Correspondence and requests for materials should be addressed to Z.V.V.

Competing financial interests

The authors declare no competing financial interests.